

Light trapping regimes in thin-film silicon solar cells with a photonic pattern

Simone Zanotto, Marco Liscidini, and Lucio Claudio Andreani*

Dipartimento di Fisica "A. Volta" and UdR CNISM, Università degli Studi di Pavia,
Via Bassi 6 I-27100 Italy

[*lucio.andreani@unipv.it](mailto:lucio.andreani@unipv.it)

Abstract: We present a theoretical study of crystalline and amorphous silicon thin-film solar cells with a periodic pattern on a sub-micron scale realized in the silicon layer and filled with silicon dioxide right below a properly designed antireflection (AR) coating. The study and optimization of the structure as a function of all the photonic lattice parameters, together with the calculation of the absorption in a single layer, allows to identify the different roles of the periodic pattern in determining an increase of the absorbance. From one side, the photonic crystal and the AR coating act as impedance matching layers, thus minimizing reflection of incident light over a particularly wide range of frequencies. Moreover a strong absorption enhancement is observed when the incident light is coupled into the quasi guided modes of the photonic slab. We found a substantial increase of the short-circuit current when the parameters are properly optimized, demonstrating the advantage of a wavelength-scale, photonic crystal based approach for patterning of thin-film silicon solar cells.

© 2010 Optical Society of America

OCIS codes: (040.5350) Photovoltaic; (050.5298) Photonic crystals.

References and links

1. J. Nelson, *The Physics of Solar Cells* (Imperial College Press, London 2003).
2. E. D. Palik, *Handbook of Optical Constants of Solids* (Academic, Orlando 1985).
3. J. Poortmans and V. Arkhipov (editors), *Thin Film Solar Cells* (Wiley, Chichester 2006).
4. P. Würfel, *Physics of Solar Cells* (Wiley-ICH, Weinheim 2005).
5. C. Heine and R. Morf, "Submicrometer gratings for solar energy applications," *Appl. Opt.* **34**, 2476 (1995).
6. M. Auslender, D. Levy, and S. Hava, "One-dimensional antireflection gratings in (100) silicon: a numerical study," *Appl. Opt.* **37**, 369 (1998).
7. C. Eisele, C. E. Nebel, and M. Stutzmann, "Periodic light coupler gratings in amorphous thin film solar cells," *J. Appl. Phys.* **89**, 7722 (2001).
8. H. Stiebig, N. Senoussaoui, C. Zahren, C. Haase, and J. Müller, "Silicon thin-film solar cells with rectangular-shaped grating couplers," *Progress in Photovoltaics: Research and Applications*, **14**, 13–24 (2005).
9. L. Zeng, Y. Yi, C. Hong, J. Liu, N. Feng, X. Duan, L. C. Kimerling, and B. A. Alamariu, "Efficiency enhancement in Si solar cells by textured photonic crystal back reflector," *Appl. Phys. Lett.* **89**, 111111 (2006).
10. K. R. Catchpole and M. A. Green, "A conceptual model of light coupling by pillar diffraction gratings," *J. Appl. Phys.* **101**, 063105 (2007).
11. K. R. Catchpole, "A conceptual model of the diffuse transmittance of lamellar diffraction gratings on solar cells," *J. Appl. Phys.* **102**, 013102 (2007).
12. P. Bermel, C. Luo, L. Zeng, L. C. Kimerling, and J. D. Joannopoulos, "Improving thin-film crystalline silicon solar cells efficiencies with photonic crystals," *Opt. Express* **15**, 16986 (2007).
13. C. Seassal, Y. Park, A. Fave, E. Drouard, E. Fourmond, A. Kaminski, M. Lemitte, X. Letartre, and P. Viktorovitch, "Photonic crystal assisted ultra-thin silicon photovoltaic solar cell," in *Photonics for Solar Energy Systems II*, A. Gombert, ed., Proc. SPIE, **7002**, 700207 (2008).

14. Y. Lee, C. Huang, J. Chang, and M. Wu, "Enhanced light trapping based on guided mode resonance effect for thin-film silicon solar cells with two filling-factor grating," *Opt. Express* **16**, 7969 (2008).
15. D. Zhou and R. Biswas, "Photonic crystal enhanced light-trapping in thin film solar cells," *J. Appl. Phys.* **103**, 093102 (2008).
16. M. Kroll, S. Fahr, C. Helgert, C. Rockstuhl, F. Lederer, and T. Pertsch, "Employing dielectric diffractive structures in solar cells—a numerical study," *Phys. Stat. Sol. A* **205**, 2777 (2008).
17. A. Chutinan and S. John, "Light trapping and absorption optimization in certain thin-film photonic crystal architectures," *Phys. Rev. A* **78**, 023825 (2008).
18. I. Prieto, B. Galiana, P. A. Postigo, C. Algora, L. J. Martinez, and I. Rey-Stolle, "Enhanced quantum efficiency of Ge solar cells by a two-dimensional photonic crystal nanostructured surface," *Appl. Phys. Lett.* **94**, 191102 (2009).
19. Y. Park, E. Drouard, O. El Daif, X. Letartre, P. Viktorovitch, A. Fave, A. Kaminski, M. Lemiti, and C. Seassal, "Absorption enhancement using photonic crystals for silicon thin film solar cells," *Opt. Express* **17**, 14312 (2009).
20. A. Chutinan, N. P. Kherani, and S. Zukotynski, "High-efficiency photonic crystal solar cell architecture," *Opt. Express* **17**, 8871 (2009).
21. R. Dewan, and D. Knipp, "Light trapping in thin-film silicon solar cells with integrated diffraction grating," *J. Appl. Phys.* **106**, 074901 (2009).
22. C. Henry, "Limiting efficiencies of ideal single and multiple energy gap terrestrial solar cells," *J. App. Phys.* **51**, 4494–4500 (1980).
23. For this reason, we refer indifferently to *microcrystalline* or *crystalline silicon*, because they have the same optical properties.
24. ASTM G 173-03, *Standard Tables for Reference Solar Spectral Irradiances: Direct Normal and Hemispherical on 37 degree Tilted Surface*, free download from <http://tredc.nrel.gov/solar/spectra/am1.5>.
25. D. M. Whittaker, and I. S. Culshaw, "Scattering-matrix treatment of patterned multilayer photonic structures," *Phys. Rev. B* **60**, 2610 (1999).
26. E. Fortunato, D. Ginley, H. Hosono, and D.C. Paine, "Transparent Conductive Oxides for Photovoltaics," *MRS Bulletin* **32**, 242–247 (2007).
27. Y. Yang, X.W. Sun, B.J. Chen, C.X. Xu, T.P. Chen, C.Q. Sun, B.K. Tay, and Z. Sun, "Refractive indices of textured indium tin oxide and zinc oxide thin films," *Thin Solid Films* **510**, 95–101 (2006).
28. M. Caglar, S. Ilican, Y. Caglar, and F. Yakuphanoglu, "The effect of Al doping on the optical constants of ZnO thin films prepared by spray pyrolysis method," *J. Mater. Sci: Mater. Electron.* **19**, 704–708 (2008).

1. Introduction

The low efficiency-to-cost ratio of solar cells is the main problem that prevents an exploitation of photovoltaics (PV) for wide-scale terrestrial applications. In commonly used crystalline silicon solar cells the active layer thickness is a few hundreds of microns [1], and the cost is dominated by silicon processing; this cost can be reduced if the high-quality active layer thickness is reduced to a few hundreds of nanometers. A variety of active materials have been explored: semiconducting polymers, CdTe, CIGS (copper indium gallium selenide) and silicon. In particular, silicon has the advantage of being fully compatible with the well-established microelectronics technology, and one possible application of optimized thin cells is the integration in chips, where the device thicknesses are limited. In such devices the etching procedures needed to realize a photonic pattern are directly comprised in the standard chip processing.

In thin-film silicon solar cells the active material can be found in both microcrystalline and amorphous form. Microcrystalline silicon has optical properties similar to those of crystalline silicon, namely an indirect gap at around 1.12 eV, and electric transport properties dominated by the presence of grain boundaries. Typical grain sizes are around 1 μm , therefore commonly employed active layer thicknesses range around that value. Amorphous silicon can be regarded as a direct gap semiconductor with an absorption threshold of about 1.25 eV [2]. In this material the diffusion length is limited to a few hundreds of nanometers; for this reason, the active layer thickness is generally limited to 300 nm [3].

Both microcrystalline and amorphous silicon thin-film cells suffer from having a large absorption length compared to active layer thickness when the incident photon energy lies in the range from the absorption threshold to about 3.5 and 2 eV, respectively. Since the solar radia-

tion, here approximated by that of a black body at a temperature of 5800 K (corresponding to 0.5 eV), has a maximum at ~ 0.8 eV in the photon flux spectrum [4], the cell must be assisted by structures that can enhance the absorption probability in the mentioned spectral range.

These structures must perform the task usually named *light trapping*: the photons must easily enter the device, where they must spend a sufficiently long time compared to the absorption time. Commercial cells currently employ antireflection (AR) coatings, back reflectors (usually Al or Ag), and patternings. Patterns are random or regular; in the last case the typical length scales are of several microns, therefore, this approach cannot be applied to thin-film cells.

Photonic crystal structures have been studied for over twenty years, as they allow to control the propagation and confinement of light at the wavelength scale and, in particular, to enhance the light-matter interaction. The application of photonic crystals in the development of solar cells to increase the light harvesting efficiency has been pioneered in a few works that delineate the fundamental concepts (Refs. [5–7]), and it has become a hot topic in the last few years (Refs. [8–21]). The structures analyzed in the literature span from very idealized to realistic ones, namely, from bare photonic crystal slabs (Refs. [13, 19]) to complete thin-film cell architectures (Refs. [16, 18, 21]). From one side, the analysis of very idealized structures is a necessary starting point, but would not fully show the advantages of patterning. From the other side, realistic structures involve many parameters (lattice constant, etching depth, fill factor . . .) in addition to electronic properties of the materials, and their study is often carried out with automatic optimization algorithms, thus making it impossible to investigate the influence of the various parameters on the cell efficiency.

Since our aim is to study the mechanisms lying behind the light coupling and trapping due to the simultaneous application of a pattern and an antireflection coating, in Sec. 2 we propose a structure that contains all the fundamental photonic components without considering the details of the charge carrier collection. The basic theory of solar cells and the numerical methods adopted, with particular regard to the calculation of absorption in a single layer of a stratified structure, are shown in Sec. 3. The numerical simulations results are shown in Sec. 4, while in Sec. 5 we investigate the mechanisms responsible for different light trapping and coupling regimes. Section 6 contains concluding remarks.

2. Structure

The structure under investigation is shown in Fig. 1(a). The silicon layer, of thickness d , lies on a silver back reflector. The top surface of silicon is etched with a one dimensional, periodic pattern of period a . In the unit cell there is a region of length b where the silicon is not etched: from this, we define the *silicon fill factor* as $f = b/a$. The etching depth is h . We also assume that the grooves left by the etching procedure are filled with silica. Above the silicon-silica pattern there is an AR layer, with thickness l and refractive index n .

This structure, reminiscent of a substrate cell architecture (see Ref. [3]), can be regarded as a generalization of the structure proposed by Seassal *et al.* in Ref. [13]: besides other tasks, here we will investigate if a shallow etching ($h < d$) can yield a cell performance comparable to the case of a deep etching ($h \simeq d$). Moreover, we will show that, as h varies from zero to about d , different coupling regimes stand out.

A silver back-reflector is taken in order to be as close as possible to the ideal metallic case (see Ref. [16] for a comparative analysis of different back-reflectors). We choose not to consider a pattern at the silicon-metal interface since the localization of the field in the (absorbing) metal grating region would limit the advantages of the increased photon path due to the pattern itself (Refs. [12, 16]). The idea of filling the air slits with SiO₂ has a twofold reason: from one side, this allows to apply on top of the patterned silicon layer an AR coating, which plays a fundamental role as impedance matching layer; from the other side, the silicon-silica interface

can act as a passivating structure preventing a strong electron-hole surface recombination.

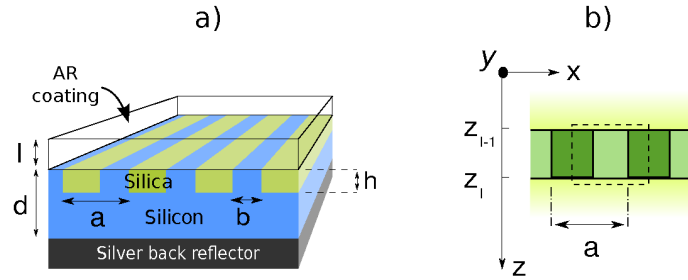


Fig. 1. (a) Structure layout and (b) integration surface for the calculation of absorption in a single layer.

3. Theoretical methods

The electric behaviour of a photovoltaic cell is fully characterized by its current-voltage curve; in particular, from that it is possible to define the efficiency of the cell. In a theoretical analysis it is usual to approximate the single junction solar cell as an ideal diode in which the generation rate has also a contribution due to the incident sunlight (Refs. [1, 4]). Adopting the explicit expressions for the I-V characteristics reported in Ref. [22], it can be shown that there is a nearly linear relation between the short-circuit current density j_{sc} (referred to as *short-circuit current* for shortness) and the efficiency. This is the reason why we choose the short-circuit current as the figure of merit.

In the approximation that each electron-hole pair generated is delivered to the external circuit, i.e., supposing that cell thickness is not larger than ambipolar diffusion length and neglecting the influence of patterning on the electrical properties of the cell [23], the short-circuit current is given by

$$j_{sc} = e \int_0^{\infty} A(E) \frac{d\mathcal{N}}{dE} dE \equiv \int_0^{\infty} \frac{dj_{sc}}{dE} dE . \quad (1)$$

With $A(E)$ we indicate the absorbance spectrum, namely the probability that a photon of energy E incident on the cell is absorbed; $d\mathcal{N}/dE$ is the number of photons incident on a unit surface area in a unit time, i.e., the photon flux, with an energy between E and $E + dE$. We define dj_{sc}/dE as *spectral contribution to the short-circuit current*. Since the absorbance is zero for photon energies below the absorption threshold E_{thr} , the integration interval has a lower limit dependent on the absorbing material. This sets a limit for the short-circuit current achievable from a cell constituted by a certain material (the limit is given by setting $A(E) = 1$ for $E > E_{thr}$); the values corresponding to crystalline and amorphous silicon are reported in Tables 1 and 2 below.

For a given structure, the short-circuit current is thus obtained integrating the absorbance spectrum weighted with the photon flux spectrum. Here we use a blackbody spectrum at a temperature of 5800 K (0.5 eV) normalized to 1000 W/m². We choose a smooth spectrum rather than the AM 1.5G spectrum [24], as our interest is to explore the light trapping mechanisms and not to obtain an overall optimized end-user commercial cell.

The absorbance spectra are calculated by means of a rigorous coupled wave method [25]. Here we give a brief description of the method, and discuss how it is possible to calculate the fraction of energy absorbed by a specific layer in the structure. The structure is supposed to

be stratified along z ; each of the layers is uniform along z and periodically patterned in the xy plane. Under these hypotheses, the electric and magnetic fields can be expanded in a Fourier series over a basis of NPW plane waves:

$$\mathbf{E}(\mathbf{R}, z) = \sum_{n=1}^{NPW} \tilde{\mathbf{E}}(\mathbf{G}_n, z) e^{i(\mathbf{k}_{\parallel} + \mathbf{G}_n) \cdot \mathbf{R}} \quad (2)$$

where $\mathbf{R} = (x, y)$; \mathbf{G}_n are the reciprocal lattice vectors and \mathbf{k}_{\parallel} is the incident wave vector component lying in the (x, y) plane. An analogous expression holds for the \mathbf{H} field. Following the notation of Ref. [25] we use

$$\begin{aligned} e_{\parallel}(z) &= [-\tilde{E}_y(\mathbf{G}_1, z) \dots -\tilde{E}_y(\mathbf{G}_{NPW}, z), \tilde{E}_x(\mathbf{G}_1, z) \dots \tilde{E}_x(\mathbf{G}_{NPW}, z)] \\ h_{\parallel}(z) &= [\tilde{H}_x(\mathbf{G}_1, z) \dots \tilde{H}_x(\mathbf{G}_{NPW}, z), \tilde{H}_y(\mathbf{G}_1, z) \dots \tilde{H}_y(\mathbf{G}_{NPW}, z)]. \end{aligned} \quad (3)$$

These are the vectors of the Fourier components of the fields that enter the solution of Maxwell equations in reciprocal space. They are obtained by propagating the field along the structure by means of a scattering matrix formalism.

Here we are interested in calculating the amount of power absorbed by a unit area of one layer in the structure. Since the structure is periodic, we limit the problem to the unit cell. By using Poynting's theorem, we calculate the Poynting vector flux over a surface enclosing the interested volume (the dashed line in Fig. 1(b) indicates that volume). The contribution of the surface facets parallel to the z direction is vanishing due to translational invariance of the system. The contribution of the surface facets normal to the z direction is simply the average of the z component of the Poynting vector over a unit cell. In general, defining the *absorbance* A_l of the l -th layer as the ratio between the power absorbed by a unit area of the l -th layer and the intensity impinging on the whole structure, the following relation holds:

$$A_l = \frac{\text{Re} \left[e_{\parallel}(z_{l-1}) \cdot h_{\parallel}^*(z_{l-1}) - e_{\parallel}(z_l) \cdot h_{\parallel}^*(z_l) \right]}{\text{Re} \left[e_{\parallel 0} \cdot h_{\parallel 0}^* \right]}. \quad (4)$$

Here, z_{l-1} and z_l are the boundaries of the l -th layer, and the subscript 0 refers to the wave impinging on the structure. The dot product is intended in the $2 \times NPW$ -dimensional reciprocal space [see Eq. (3)]. By summing up the contributions of all the layers of interest, one can calculate the absorbance in a desired region of the multilayer structure. This approach works with both transparent and absorbing substrates, and allows one to avoid time consuming field integrations.

4. Numerical results

In this section we show the dependence of the short-circuit current on the parameters of the structure and the configurations that maximize it. The analysis is carried on separately for crystalline and amorphous silicon. In both cases we consider two silicon layer thicknesses: $d = 500$ and 1000 nm for c-Si, $d = 100$ and 300 nm for a-Si. These values are chosen to take into account the typical diffusion lengths in the materials. The refractive indices of all materials (c-Si, a-Si, SiO_2 , and silver) are frequency-dependent and have been taken from Ref. [2].

4.1. Crystalline silicon

Crystalline silicon is an indirect gap semiconductor, with $E_g = 1.12$ eV. Although the absorption threshold is somewhat lower than this value because of the *Urbach tail* [1], the absorption

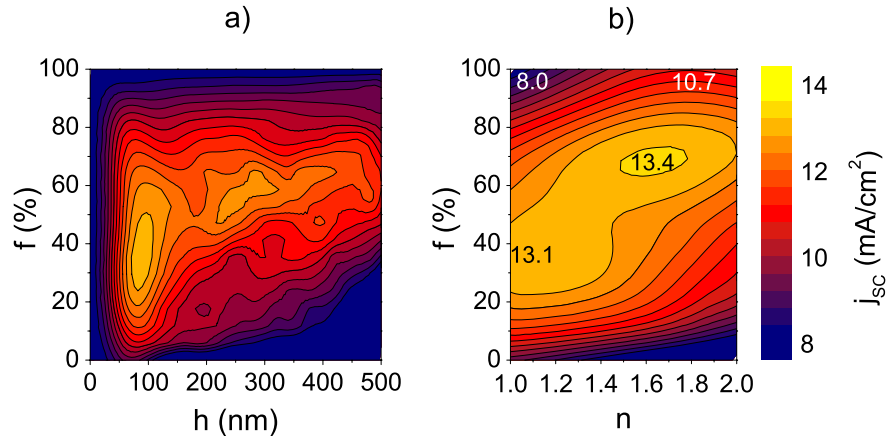


Fig. 2. (a) Short-circuit current dependence on the etching depth h and the silicon fill factor f . The absorbing layer is c-Si with a thickness $d = 500$ nm, the lattice parameter is $a = 450$ nm and there is no AR coating. (b) Short-circuit current dependence on the refractive index n of the AR coating and on the silicon fill factor f . The parameters d and a are the same as in (a), the etching depth is fixed at 80 nm and the AR coating thickness is $l = 70$ nm.

coefficient is very small below E_g . Thus, in our simulations, we consider the spectral region above 1.12 eV. The upper limit is taken to be 3.5 eV, as above this value the solar photon flux is negligible and the absorbance is essentially independent of any pattern. By considering the absorbance $A(E) = 1$ in the mentioned spectral region, we obtain the ideal limit for the short-circuit current $j_{sc} = 36.4$ mA/cm².

First we consider a c-Si structure with silicon thickness 500 nm. In the case of a bare slab without pattern and without AR coating, but with the sole back reflector, the short-circuit current is only 8.0 mA/cm². On the other hand, if we consider an unpatterned silicon slab with an optimized AR coating ($n = 1.9$, $l = 70$ nm, Ref. [12]) in addition to the back reflector, we can reach $j_{sc} = 10.7$ mA/cm². This is the value that we take as our reference to evaluate the efficiency enhancement given by the introduction of a photonic pattern.

The first analysis consists in varying simultaneously the etching depth h and the fill factor f for a cell without the AR coating. The result is shown in Fig. 2(a) for a period $a = 450$ nm. The calculations performed for $a = 300$ and 600 nm show qualitatively similar results, although the maximum j_{sc} is smaller; the reason for this can be understood by considering the number of allowed diffracted waves in air and silicon as the pattern period varies. Indeed, when $a = 300$ nm, there is no diffracted light lost in the air (the first diffraction channel opens at 4.13 eV), but also the silicon supports few diffracted waves. When a is large, say 600 nm, there are many diffraction orders in the silicon, but part of the incident light is diffracted back to the air (the first diffraction channel opens at 2.07 eV) The trade-off between increasing the diffraction in silicon and limiting that in air gives, for the solar spectrum considered, an optimized period $a = 450$ nm. This parameter is fixed in all the following simulations.

The analysis of Fig. 2(a) shows that there are two maxima: one at $h = 80$ nm, $f = 35\%$ with $j_{sc} = 13.1$ mA/cm², and the other one at $h = 300$ nm, $f = 60\%$ with $j_{sc} = 12.4$ mA/cm². By considering the h values, we name these situations *shallow etching* and *deep etching*, respectively. In both cases the short-circuit current shows a considerable improvement with respect to the reference system. The origin of the two maxima is an optimization of the coupling efficiency of the incident light: the underlying mechanism will be discussed in Sec. 5.1.

A further increase in the short-circuit current may be achieved by adding an AR coating directly on the patterned layer. We first attempted to optimize the coating parameters – refractive index n and thickness l – while keeping the fill factor and the etching depth fixed at the shallow etching optimal configuration (that is $h = 80$ nm, $f = 35$ %). This strategy does not result in an appreciable improvement of the cell performance.

The complicated task of optimizing the short-circuit current should be faced by exploring the whole parameter space, i.e., letting all the parameters simultaneously vary. However, it is possible to obtain good results also by first optimizing a certain group of variables, and then the remaining ones. The following procedure was found to be satisfactory: we first set the etching depth at the optimal value for the *shallow etching* configuration ($h = 80$ nm), then look for a maximum by simultaneous variation of f and n , and eventually optimize l . The simultaneous optimization of f and n allows to take into account the interplay of the grating and the coating, i.e., of the photonic pattern that has the role of optimizing light harvesting and of the AR coating that minimizes the reflection losses.

The result of the simulation is reported in Fig. 2(b). On the upper side of the domain, where $f = 100$ %, the situation is that of an unpatterned structure with an AR coating, while the left side refers to a patterned structure without AR coating: this parameter range contains some of the relevant configuration seen before and a new interesting one. The structure corresponding to the upper left corner is the bare silicon slab, whose short-circuit current is 8.0 mA/cm². When $f = 100$ % and $n = 1.9$ the situation is that of an optimized AR coating over an unpatterned slab with $j_{sc} = 10.7$ mA/cm², while the configuration $f = 35$ %, $n = 1$ corresponds to the optimal patterning found when no AR is applied. An overall increase of the short-circuit current can be found by looking at the center of the parameter space, where $f = 70$ % and $n = 1.7$, with $j_{sc} = 13.4$ mA/cm². The analysis of the contour plot shows that a separate optimization of f and n would not work. Indeed, if f is first fixed to the optimal value for an uncoated structure, the sole variation of n does not allow to explore the region of the maximum, as the parameters f and n are correlated.

The dependence on the AR coating thickness l has been studied by realizing similar plots. They showed the same correlation between f and n , the same position of the maximum with a slight variation in the maximum achievable short-circuit current; $l = 70$ nm is the optimal value.

A similar analysis can be carried out when fixing $h = 300$ nm (*deep etching*). However, in this case we do not find a strong correlation between f and n , and the optimal parameters are $f = 60$ %, $n = 1.6$; the short-circuit current is 14.6 mA/cm². These results seem to indicate that, after an optimization of the cell parameters, the maximum short-circuit current is obtained for a deep-etched grating. However, we observe that this value is still very close to that of the optimized shallow-grating structure. In practice, a deep-etching structure could suffer from higher recombination losses that are not considered here; thus, the shallow-etched structure may offer the best compromise between increase in short-circuit current and overall optimization of the structure.

The spectral contribution to the short-circuit current calculated for most of the structures previously mentioned are shown in Fig. 3(a). Comparing curves (1) and (2), it can be seen that the application of an AR coating on top of an unpatterned structure plays an important role above 2 eV, while the spectral region between 1.12 and 2.75 eV is strongly affected by the patterning [curves (3) and (4)]; above 2.75 eV the patterned structure behaves similarly to the unpatterned coated structure. The difference between shallow etching (3) and deep etching (4) is limited to the energies below 2 eV. In the spectral region above 2.5 eV the patterned cells behave almost like an ideal absorber, therefore, a further increase in the short-circuit current can be achieved only by acting on the spectral region [1.12, 2.5] eV. Note that the spectra

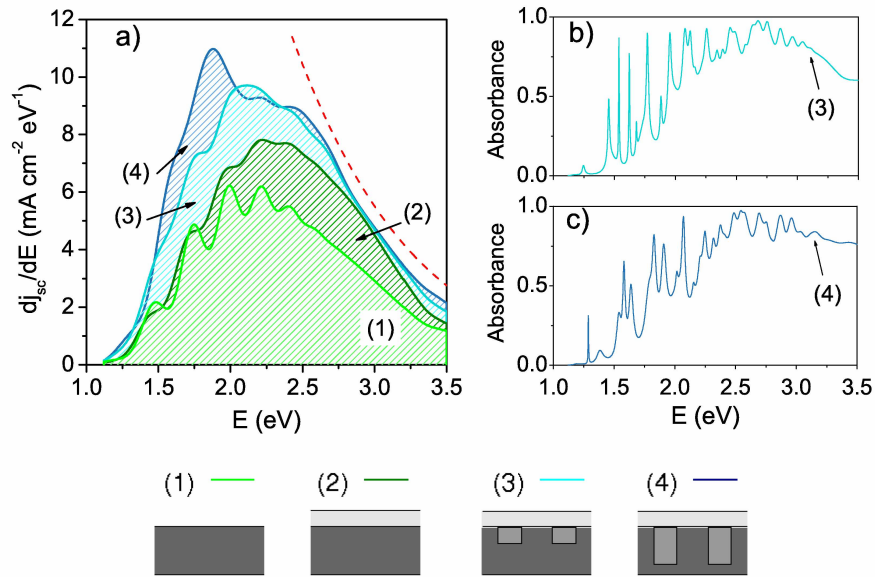


Fig. 3. (a) Spectral contribution to the short-circuit current as a function of the incident photon energy for several c-Si structures. Light is unpolarized and at normal incidence. The thickness of the silicon layer is always 500 nm. The structures are: (1) unpatterned without AR coating; (2) unpatterned with AR coating; (3) shallowly patterned with AR coating; (4) deeply patterned with AR coating (see also Table 1). For the readability of the figure, the curves are smoothed by means of a convolution with a Gaussian having standard deviation $\sigma = 0.075$ eV. The red dashed line refers to the ideal absorber. (b) and (c) Absorbance spectra for structures (3) and (4), respectively. Light is at normal incidence and the electric field is polarized parallel to the stripes; the spectra are not smoothed.

are smoothed for better readability of the figure (see caption), but the short circuit current is calculated with the original spectra.

The bare absorbance spectra for the shallow- and deep-etched structures are shown in Fig. 3(b) and 3(c), respectively. In both cases the region between 1.12 and 2.5 eV contains several sharp peaks, that are associated with the coupling of the incident light to the quasi-guided modes of the silicon slab, as also found for other structures (Refs. [12–19]). In this spectral region the mean absorbance is quite below unity, because of the very low absorption coefficient of the crystalline silicon.

By proceeding in the same way as described above, we carried on the study of a c-Si cell having thickness $d = 1000$ nm. The results, qualitatively similar to those concerning the thickness $d = 500$ nm, are reported in Table 1. In conclusion, we note that the short-circuit current values are still quite far from the theoretical limit, but the patterning allows to achieve significant increments of the short-circuit current. The patterned layer increases light absorption within silicon and also (due to its reduced average refractive index) it improves the impedance matching between air and the underlying homogeneous silicon, however the combination of a photonic patterning and a carefully optimized AR coating allows to achieve higher increments of the short-circuit current, in particular for the thickness $d = 500$ nm.

Table 1. Short-circuit currents values for several c-Si structures (bold face, expressed in mA/cm²). The percentages show the variation with respect to the unpatterned structure with AR coating; all the calculations have been carried out on the range [1.12, 3.5] eV. The numbers in parentheses refer to the convention used in Fig. 3.

Active layer thickness d	500 nm	1000 nm
No pattern, no AR coating (1)	8.0	10.6
No pattern, AR coating (2)	10.7	14.6
	$n = 1.9$ $l = 70$ nm	$n = 1.9$ $l = 70$ nm
Optimized shallow pattern without AR coating	13.1 +22.5 %	16.4 +12.4 %
	$h = 80$ nm $f = 35$ %	$h = 80$ nm $f = 25$ %
Optimized deep pattern without AR coating	12.4 +15.0 %	14.9 +2.0 %
	$h = 300$ nm $f = 60$ %	$h = 800$ nm $f = 60$ %
Optimized shallow pattern with AR coating (3)	13.4 +25.5 %	18.6 +27.0 %
	$h = 80$ nm $f = 70$ % $n = 1.7$ $l = 70$ nm	$h = 80$ nm $f = 60$ % $n = 1.6$ $l = 80$ nm
Optimized deep pattern with AR coating (4)	14.6 +36.5 %	17.8 +21.9 %
	$h = 300$ nm $f = 60$ % $n = 1.6$ $l = 70$ nm	$h = 800$ nm $f = 70$ % $n = 1.8$ $l = 70$ nm
Ideal c-Si absorber	36.4 (limiting value for j_{sc})	

4.2. Amorphous silicon

The analysis of the amorphous silicon solar cell is carried on for the same cell geometry, but the thickness is now chosen to be $d = 300$ nm, as imposed by the shorter carrier diffusion length. Since the absorption threshold is 1.25 eV, the spectral range spanned in the calculation is [1.25, 3.5] eV; the ideal limit for the short circuit current is now $j_{sc} = 31.9$ mA/cm².

In Fig. 4(a) we show the dependence of the short-circuit current on etching depth and fill factor for an uncoated cell. As in the crystalline silicon case, there are two maxima occurring for shallow and deep etching. In this case, the deep etching maximum occurs very close to a full etching situation ($h = 280$ nm). In Fig. 4(b) we show the dependence of j_{sc} on f and n . This result is similar to that observed for the c-Si cases, and the maximum still lies in the middle of the parameter space. As in the c-Si case, it can be shown that the lattice parameter has a small influence on the result, and the optimal value is still $a = 450$ nm.

Figure 5 shows the spectral contributions to the short-circuit current and the absorbance spectra. While the calculation of j_{sc} is done considering the range [1.25, 3.5] eV, the most important spectral features lie in the spectral region below 2 eV. From the comparison of curves (1) and (2) in graph (a), we can appreciate the importance of an AR coating on most of the spectral range; the effect of the pattern [curves (3) and (4)] is to slightly increase dj_{sc}/dE in the interval [1.3, 1.6] eV. Above 1.75 eV the a-Si cells behave like an ideal absorber. The features in the spectra of the patterned structures can be read from Fig. 5(b) and 5(c), where no smoothing has been performed. The spectrum of the shallow-patterned structure [curve (3)] shows a few weak shoulders; when the etching is deep [curve (4)] they evolve into two wide peaks.

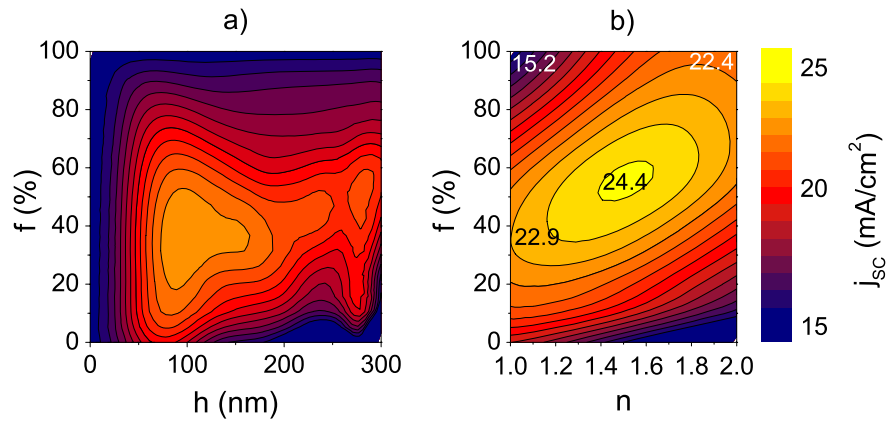


Fig. 4. (a) Short-circuit current dependence on the etching depth h and the silicon fill factor f . The absorbing layer is a-Si with a thickness $d = 300$ nm; there is no AR coating. (b) Short-circuit current dependence on the refractive index n of the AR coating and on the silicon fill factor f . The absorbing layer is the same as in (a), the etching depth is fixed at 100 nm and the AR coating thickness is $l = 80$ nm.

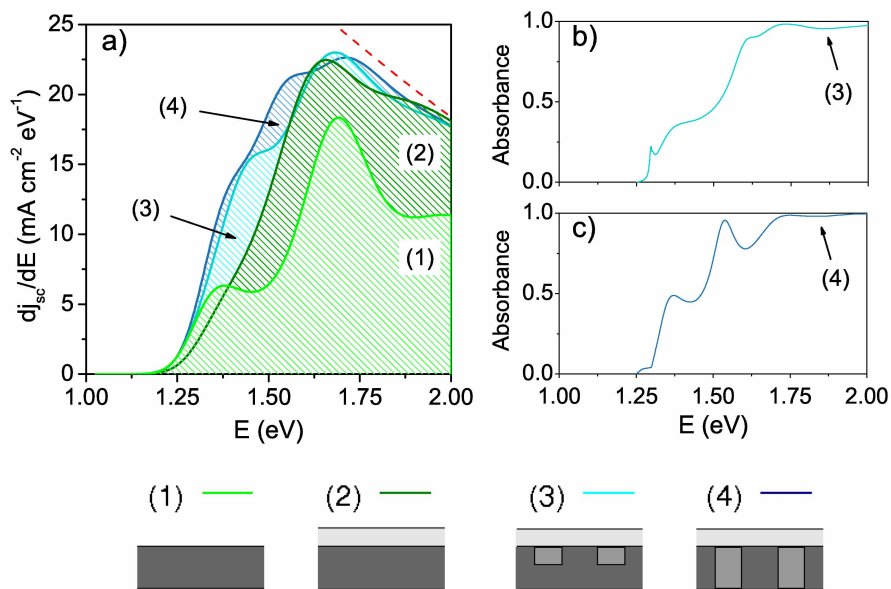


Fig. 5. (a) Spectral contribution to the short-circuit current as a function of the incident photon energy for several a-Si structures. Light is unpolarized and at normal incidence. The thickness of the silicon layer is always 300 nm. The structures are: (1) unpatterned without AR coating; (2) unpatterned with AR coating; (3) shallowly patterned with AR coating; (4) deeply patterned with AR coating (see also Table 2). For better readability of the figure, the curves are smoothed by means of a convolution with a Gaussian having standard deviation $\sigma = 0.05$ eV. The red dashed line refers to the ideal absorber. (b) and (c) Absorbance spectra for structures (3) and (4), respectively. Light is at normal incidence and the electric field is polarized parallel to the stripes; the spectra are not smoothed.

Table 2. Short-circuit currents for several a-Si structures (expressed in mA/cm²). The percentages show the variation with respect to the unpatterned structure with AR coating; all the calculations have been carried out on the range [1.25, 3.5] eV. The numbers in parentheses refer to the convention used in Fig. 5.

Active layer thickness d	100 nm	300 nm
No pattern, no AR coating (1)	13.2	15.2
No pattern, AR coating (2)	19.3	22.4
	$n = 2.0$ $l = 60$ nm	$n = 1.9$ $l = 70$ nm
Optimized shallow pattern without AR coating		23.0 +2.37 %
		$h = 100$ nm $f = 35$ %
Optimized deep pattern without AR coating	18.4 -4.80 %	21.3 -4.9 %
	$h = 90$ nm $f = 60$ %	$h = 280$ nm $f = 50$ %
Optimized shallow pattern with AR coating (3)		24.4 +8.84 %
		$h = 100$ nm $f = 60$ % $n = 1.6$ $l = 80$ nm
Optimized deep pattern with AR coating (4)	21.7 +12.4 %	25.0 +11.3 %
	$h = 90$ nm $f = 60$ % $n = 1.6$ $l = 80$ nm	$h = 280$ nm $f = 60$ % $n = 1.6$ $l = 80$ nm
Ideal a-Si absorber	31.9 (limiting value for j_{sc})	

A summary of the results for the a-Si structure with a thickness of the active layer $d = 300$ nm, and the analogous results for a 100 nm thick structure, are given in Table 2. When considering a thickness of 100 nm there is no shallow etching regime: the analogous of Fig. 4(a) would show a single maximum centered around the etching depth $h = 90$ nm. In this case the simple patterning without any AR coating results in a decrement of the short-circuit current with respect to the reference structure. A similar decrement is also found for the 300 nm thick structure. Nonetheless, in both cases, the simultaneous presence of a pattern and an AR coating gives rise to an increase of more than 10 % in the short-circuit current.

5. Discussion of results

A patterned solar cell can be regarded as constituted by different photonic components, which participate with different mechanisms to light collection. Here we first show the features of the coupling regimes due to different etching depths, and then we apply effective medium theory to the silicon-silica pattern.

5.1. Coupling regimes

Let us consider the geometry reported in Fig. 1(a), without any AR coating. When there is no pattern, since the silicon thickness d is comparable to the light wavelength, the device is just an asymmetric slab and its absorbance spectrum is dominated by the Fabry-Pérot resonances.

In the presence of a shallow periodic etching ($h \ll d$), the slab guided modes are slightly perturbed, and the grating makes them accessible from an incident radiation. A simple picture

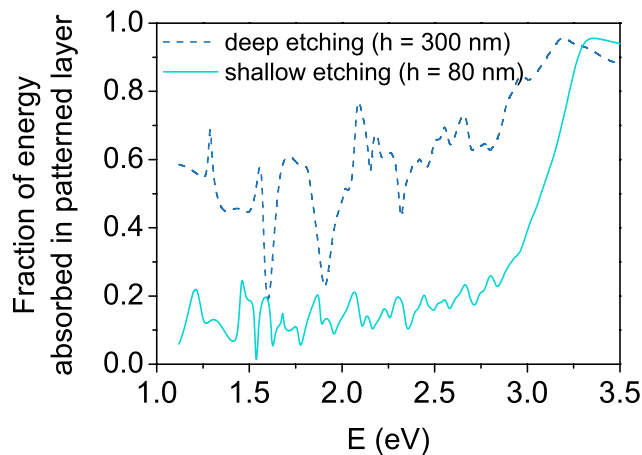


Fig. 6. Fraction of energy absorbed in the patterned layer of thickness h for TE polarization, calculated for two different c-Si structures.

often found in the literature recognizes in our silicon-silica pattern a diffraction grating, which deviates the normally incident light ray to an oblique direction, thus increasing the path in the absorbing material. According to this model, at the opening of a diffraction channel each diffracted wave propagates at nearly grazing angles within the material, with a large propagation path - which explains the increased absorption due to the grating [difference between curves (3) and (2) in Fig. 3(a)] over a wide spectral range. However, since we are considering a thin-film cell with a sub-micrometric pattern, ray optics is not directly applicable. The role of the grating is to couple the incident radiation field to the guided slab modes, without substantially modifying the modes themselves. The openings of successive diffraction channels, together with the Fabry-Pérot resonances in the slab, are responsible for the complex peak structure in Fig. 3(b).

When the etching depth becomes comparable to the slab thickness ($h \simeq d$), the slab modes are substantially modified. In this last situation, often referred in the literature as *photonic crystal (PhC) slab*, the absorbance spectrum will show peaks correspondent to the crystal modes that can be excited by an incoming radiation (see also Ref. [17]). The influence of the etching depth on the position and shape of the resonances can be read out by comparing Figs. 3(b) and 3(c).

In the analysis of the crystalline silicon structure of thickness 500 nm (Sec. 4.1), we labelled as *deep etching* the case $h = 300$ nm. In Fig. 6 we report the fraction of energy absorbed in the layer of thickness h where silicon alternates with silica [*patterned layer*, see Fig. 1(a)]. Considering the region below 3 eV, the spectrum correspondent to the deep etching configuration has an average value higher than 0.5, while for the shallow etching configuration the fraction of absorbed energy in the patterned layer is no more than 0.15 on the average: this indicates that for the case of shallow etching the patterned layer has the only function of coupling the radiation with the underlying bulk silicon layer, where most of the absorption takes place.

The deep etching configuration is complicated, as it does not represent a pure photonic crystal slab configuration, rather a PhC slab coupled with an unpatterned slab. In the case of the deep etching configuration the fraction of absorbed energy in the patterned layer shows strong oscillations with pronounced peaks and dips. These oscillations point to an alternation of modes concentrated in the patterned layer or in the underlying silicon layer. To clarify this point we show in Fig. 7 the electric field intensities for six different energies that represent peaks [(a)

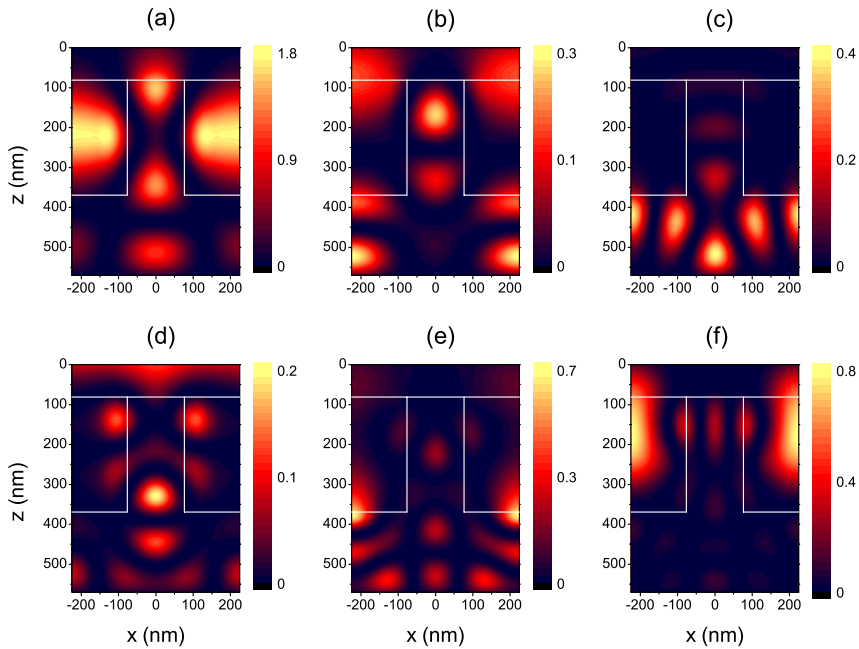


Fig. 7. Electric field intensities for the deeply etched c-Si structure of Fig.6 ($h = 300$ nm) for TE polarization, calculated for the following energies: (a) $E = 1.287$ eV, (b) $E = 1.385$ eV, (c) $E = 1.600$ eV, (d) $E = 1.726$ eV, (e) $E = 1.910$ eV, and (f) $E = 2.090$ eV.

and (f)], plateaus [(b) and (d)] and dips [(c) and (e)] in the dashed curve of Fig. 6. It can be verified that the field intensity is higher in the patterned region in correspondence with the peaks in Fig. 6, while it is higher in the unpatterned region in correspondence with the dips. This confirms that in the energy range below 3 eV, the enhancement of spectrally integrated absorption for the deep etching configuration has significant contributions from both patterned and unpatterned silicon regions. When the photon energy is above $\simeq 3$ eV, energy absorption takes place in the upper layer for both deep- and shallow-etched structures, as the absorption coefficient is strong.

5.2. Effective index

In the spectral region where the wavelength is larger than the lattice constant, the light does not experience the silicon-silica pattern as a diffraction grating, rather as an uniform material whose dielectric constant is a weighted average of the dielectric constants of silicon and silica. This behaviour can be quantified by recalling the expression for the *effective index* of an arrangement of dielectric slices. Referring to the Fig. 1(a) for the notation, the average over the polarizations reads (notice that we are at normal incidence):

$$\epsilon_{eff}(f) = \frac{1}{2} \left[f \epsilon_{Si} + (1-f) \epsilon_{SiO_2} + \frac{1}{f/\epsilon_{Si} + (1-f)/\epsilon_{SiO_2}} \right]. \quad (5)$$

When an AR coating is applied over the patterned structure, in order to match the impedance of the air with that of the effective layer, the usual optimal matching condition gives the relation between the AR coating refractive index n and the silicon fill factor f :

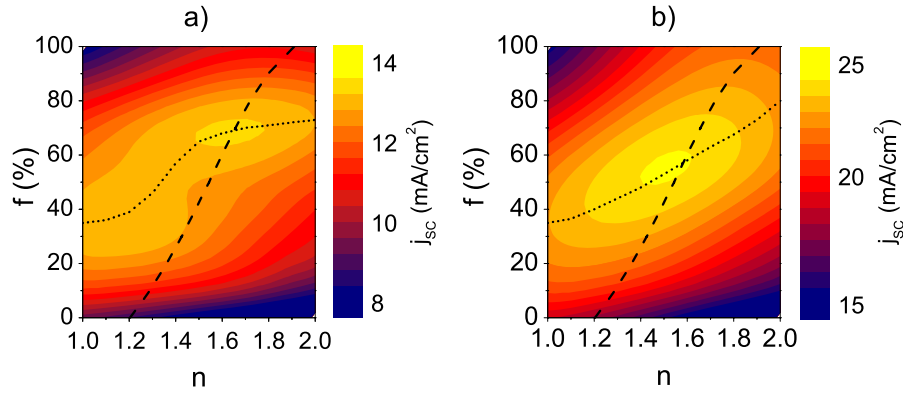


Fig. 8. Correlation between silicon fill factor f and AR coating refractive index n : comparison of numerical data (colour map: dependence $j_{sc}(f, n)$); dash line: steepest descent curve starting from the best uncoated configuration) and effective-index analytical result (dash-dot line). (a) refers to c-Si, (b) refers to a-Si [see also Figs. 2 (b) and 4 (b)].

$$n(f) = [n_{eff}(f)]^{\frac{1}{2}} = [\epsilon_{eff}(f)]^{\frac{1}{4}}. \quad (6)$$

The correlation obtained between f and n can be compared with the results of the numerical analysis of the dependence of j_{sc} on f and n . The contour plots reported in Figs. 2(b) and 4(b) are redrawn in Fig. 8, with superimposed (dotted line) the steepest curve starting from the optimal unpatterned configuration ($f = 35\%$, $n = 1$). The analytical curve expressed by the relations (5) and (6) is reported as a dashed line. Since the maximum spectrally integrated short-circuit current for the unpatterned layer ($f = 100\%$) is obtained with an AR coating with $n = 1.9$ (see also Tables 1 and 2), the refractive index of c-Si and a-Si to be used in Eq. (5) has been fixed to $n_{Si} = 1.9^2 = 3.61$. We interpret the difference between dotted and dashed lines as a consequence of the fact that the pattern action goes beyond the simple effective mean approximation. Indeed, the short-circuit current results from an integration over a wide spectral range, where the diffractive action of the patterning is not negligible. Nonetheless, it is interesting to notice that in both cases of crystalline and amorphous silicon the lines cross exactly at the absolute maximum of the function $j_{sc}(f, n)$. Also, the main trend is reproduced, indicating that a coarse optimization of the AR coating in related (even more complex) structures can still be attempted by an effective-index approximation.

5.3. Anti-reflection coating

Since the maximum increase in short-circuit current depends on a careful choice of photonic lattice parameters and of the refractive index and thickness of the AR coating, it is important to discuss possible materials that could be used for the AR coating. Usually, transparent conductive oxides (TCOs) are employed as AR coatings as they also act as electrode elements which facilitate metallic contacting [26]. However, the most commonly employed Indium Tin Oxide (ITO) has a refractive index ranging between 1.9 and 2.2 [27], which is higher than the optimal values found in Sec. 4.

When looking for appropriate AR coating materials it is useful to discuss the change of the short-circuit current with the AR coating refractive index, i.e., the tolerance of the maximum

j_{sc} with respect to variations in n . By analyzing the numerical results reported in Figs. 2(b) and 4(b), it turns out that the maximum j_{sc} changes by less than a percent for n ranging from 1.5 to 1.8 in the case of crystalline silicon, and from about 1.4 to 1.6 in the case of amorphous silicon, respectively. Among the TCOs, Al-doped Zinc Oxide (AZO) could be the most appropriate material as the effect of Al doping on ZnO yields a refractive index between 1.5 and 2, depending on wavelength and Al concentration [28]. Clearly a detailed study of actual cell architecture including metallic contacts should be made, which goes beyond the scope of the present paper.

Another interesting possibility would be to use the same material for the AR coating and for filling the photonic pattern. Although in this case the AR coating would probably be not fully optimized, this solution would combine easier realization with better charge collection properties of the cell. The optical performance of this kind of structure could be studied by performing calculations similar to those of the present paper, nevertheless a detailed investigation of actual cell architecture including optical and electrical properties would again be very helpful and this can be the direction for extending the present work towards real PV cell structures.

6. Conclusions

In this work we analyzed the influence of the application of a submicrometer pattern and an antireflection coating on a thin-film solar cell with crystalline or amorphous silicon as absorber material. By varying the structure parameters we found the possibility of a significant increase of the short-circuit current j_{sc} , with respect to an unpatterned cell with an optimized AR coating. This study was carried out over a wide spectral range, using a rigorous coupled-wave approach to describe the optical properties of the structures. Although the electronic properties have not been taken into account in our discussion, the thicknesses of the silicon layer we have considered are realistic in terms of the typical carrier diffusion lengths in a-Si and c-Si. Moreover, the silica filling of the photonic pattern we are proposing is meant to minimize the carrier surface recombination losses.

The optimization process has been carried out by exploring the dependence of the short-circuit current upon one or two parameters at a time. Even though a full multiparameter optimization could lead to a slightly higher maximum, we found significant increases of j_{sc} , and we had the possibility to have an insight into the physics governing the light trapping mechanisms. We pointed out the presence of two different coupling regimes: (1) When the pattern is shallow and the guided modes of the silicon slab are only slightly perturbed, (2) When the pattern is deep and the system behaves as a photonic crystal slab. Moreover, we recognized that the pattern layer acts also as an impedance matching layer, and we described this effect in the framework of an effective medium theory with fair agreement.

We found improvements of up to 12.4 % for an amorphous silicon structure, and up to 36.5 % when crystalline silicon is the absorbing material, relative to the reference unpatterned structures with an optimized AR coating. We also noticed that a shallow etching configuration gives the best compromise between increase in the short-circuit current and overall feasibility and performance of the structure. These results confirm an advantage of a wavelength-scale photonic crystal based approach, to improve the performances of thin-film solar cells.

Acknowledgments

We are grateful to C. Seassal for sending us Ref. [19] prior to publication and for useful correspondence. Helpful discussions with M. Patrini are also gratefully acknowledged. This work was supported by CNISM through the INNESCO initiative and by Fondazione Cariplo through project 2007-5259.